Hindawi
Advances in Civil Engineering
Volume 2019, Article ID 2709890, 8 pages
https://doi.org/10.1155/2019/2709890

Research Article

Rotational Restraint to Purlins Provided by Standing Seam Roof Systems

Qin Yang,[1] Wei Luan,[2] Shaole Yu,[2] and Junjie Chen[2]

[1]*East China Architectural Design & Research Institute Co., Ltd, Shanghai 200011, China*
[2]*China Construction Eighth Engineering Division Co., Ltd., Shanghai 200135, China*

Correspondence should be addressed to Wei Luan; lwei13@163.com

Received 19 July 2019; Accepted 3 December 2019; Published 23 December 2019

Academic Editor: Tayfun Dede

The finite element model used for analyzing the rotational restraint rigidity of standing seam roof systems was developed. The influences of different factors on the rotational restraint rigidity provided by two types of standing seam roof systems were studied. The variables include local deformation of standing seam roof panels, panel thickness, clip tab thickness, and the relative sliding of clip tab and clip base. The restraint mechanism of standing seam roof systems to the purlins was studied. It is shown that the rotational restraint rigidity provided by the two types of researching standing seam roof systems mainly depends on the slide tab thickness and the roof panel thickness. Finally, formulae for calculating rotational restraint rigidity of the LSIII and SS360 standing seam roof systems were also proposed based on parametric analysis results.

1. Introduction

Cold-formed purlins are widely used in metal buildings due to their economy, ease of fabrication, and high strength-to-weight ratios. However, these sections are weak in the lateral direction and in torsion [1]. Previous work shows that conventional roof panels which are directly through-fastened to purlins by self-drilling screws can provide full lateral bracing and some extent of rotational restraint to the purlins by virtue of their shear rigidity and resistance to local bending at the connections [1–5]. In order to accurately calculate the uplift capacity of purlins with top flange through-fastened to roof panels, a series of tests were conducted by several scholars [1–11] to determine the rotational restraint to purlins provided by the purlin-panel systems, and the test set-up and procedure were proposed by Celebi et al. [1], improved by Pekoz et al. [3], and adopted by Eurocode 3-1-3 [12]. Katnam et al. [13, 14] developed a nonlinear finite element model to estimate the rotational restraint provided by the first and second generation trapezoidal sheeting to the attached purlin. The model was applicable to trough-fixed and crest-fixed single skin purlin-sheeting systems, and the performance of which was validated to be in good agreement with test results. It opened the way to the development of a design method for estimating the rotational restraint provided by the sheeting to cold-formed steel purlins. To determine the rotational restraint that sheathing provides to the flange of a cold-formed steel floor joist or stud, a series of cantilever tests on joist/stud-sheathing assemblies were conducted by Schafer [15, 16]. The tests demonstrated that the rotational stiffness may be decomposed into two parts: connector and sheathing. The connector stiffness was due to the rotation of the fastener in the flange of the cold-formed steel member and was most significantly influenced by the thickness of the cold-formed steel member itself. The sheathing stiffness was due to bending of the sheathing itself and may be highly variable. The results formed the basis for a new design method adopted in American standards (AISI-S210-10) [17] for incorporating restraint into design strength predictions for the distortional buckling mode. Gao and Moen [18, 19] proposed mechanics-based equations for predicting the rotational restraint provided by through-fastened metal panels to Z- and C-section girts or purlins. The prediction equations were validated by conducting rotational restraint experiments, and the through-fastened connection stiffness

was also simulated in a finite strip elastic buckling analysis with a rotational spring to demonstrate how system effects can be included in design.

In recent years, standing seam roof systems are very prevalent since they are well adapted to the thermal expansion and contraction deformation caused by temperature changes. In these roof systems, standing seam roof panels are fastened to purlins through sliding clips, so that movement of roof panels relative to the purlins is permitted. Therefore, the behavior of purlins in these roof systems is directly related to the rotational restraint provided by the standing seam roof systems. Liu et al. [20] studied the rotational restraint to purlins provided by standing seam roof systems through 28 groups of tests, and it was confirmed that the total rotational rigidity of standing seam roof systems is formed by connecting the rotational rigidity of roof panels, clips, and purlins in series. However, because there are many types of standing seam roof systems, and the roof panel profile, standing seam configuration and sliding clip details are different, and it is difficult to determine all of the rotational restraints provided by these roof systems through tests. So far, the rotational restraint rigidity to purlins provided by the LSIII and SS360 standing seam roof systems has not been specially studied. Thus, in this paper, the rotational restraint to purlins provided by two types of standing seam roof systems widely used in China was analyzed using finite element models, and the influence factors were also investigated and formulae for calculating rotational restraint rigidity were also proposed and verified.

2. Research Object

Two types of standing seam roof systems widely used in China were taken as the research objects. One type was the LSIII standing seam roof system consisted of LSIII standing seam roof panels fastened to the purlins with LS003 clips. Another type was SS360 standing seam roof system consisted of SS360 standing seam roof panels fastened to the purlins with S3PC-1 clips. Both of these roof panels, although from different manufacturers, had very similar profiles. The panel sidelaps were mechanically seamed in the field to form the 450° and 360° seams for LSIII and SS360 roof systems, respectively. The yield stress of both roof panels as reported by the manufacturers was 345 MPa, and the mean measured thickness including coating was 0.6 mm. The LS003 clip was composed of a clip base 2.0 mm in thickness and a slide tab 1.0 mm in thickness, the slide tab was 110 mm in length and attached to the clip base with an interlocking design that permits relative movement between them. The S3PC-1 clip consisted of an L-shaped clip base 2.6 mm in thickness and a thinner slide tab (0.8 mm in thickness), the L-shaped clip base was 115 mm in length with a rectangular slot on the vertical plane, the slide tab was attached to the clip base at the slotted interface, which allows the movement of the slide tab within the confines of the slot length (91 mm). Both the clip bases were fastened to purlins with two self-drilling screws, and the dimensions and connection details are shown in Figures 1–3. Z-purlins were used in the experimental program. The angle between the lip and flange is 45° for all the Z-sections. The cross-section dimensions of the purlins (height, flange width, and thickness) varied between tests.

3. Finite Element Analysis

Using the general purpose finite element analysis (FEA) program ANSYS, finite element models used for calculating the rotational restraint rigidity provided by standing seam roof systems were developed according to [20], nonlinear analysis was performed, and the rotational restraints on purlins provided by the two types of standing seam roof systems were also analyzed.

3.1. Finite Element Models. As shown in Figure 4, the finite element model consisted of 3 pieces of roof panels supported by two lines of purlins at ends with one row of clips connected at the midspan of the roof panels. A pair of concentrated forces with same value and opposite direction was applied at two screw connection points of each clip base to simulate the torque transmitted from the purlin.

The standing seam roof panels and clips were modeled using the SHELL 181 element, which is a 4-node shell element with six degrees of freedom at each node. And based on reasonable consideration of the stress stiffening, large rotation, and large strain, the SHELL 181 element is well suited for analyzing thin to moderately thick shell structures. The finite element mesh size of the models was investigated to provide both accurate and time-efficient results. The standing seam roof panels and clips were all modeled as nonlinear materials using the ideal elastic-plastic model, the yield stress of which was obtained from product reports provided by the manufacturers. The full-scale tests on wind uplift capacity of purlins supporting the standing seam roof systems presented by Luan and Li [21, 22] showed that the mechanical seams of the panel sidelaps were fixed tightly, and no failure or separation were observed. Therefore, the translation freedoms of the corresponding nodes between the panels and the slide tabs were also coupled as shown in Figure 5. Considering that the movement distance of the slide tab relative to the clip base was generally not very large in the tests, to simplify the finite element model, it is assumed that no relative movement had occurred between the slide tab and clip base; therefore, along the longitudinal direction of the roof panel, the translation freedom of the corresponding nodes was also coupled. The influence of the relative movement was also specially studied. The standing seam roof panels were supported by two C-purlins at the ends, and the roof panels were connected with purlins through sliding clips, so the translation freedoms of the corresponding nodes between the clip base and supporting purlins were also coupled. The purlins were assumed to be simply supported, to simulate the boundary condition, and at both ends of each purlin, the translation in the vertical direction of the central point and the translations in the lateral direction of the web line points were constrained. The translation in the longitudinal direction of the central point at one end of the purlin was also constrained to avoid rigid body displacement.

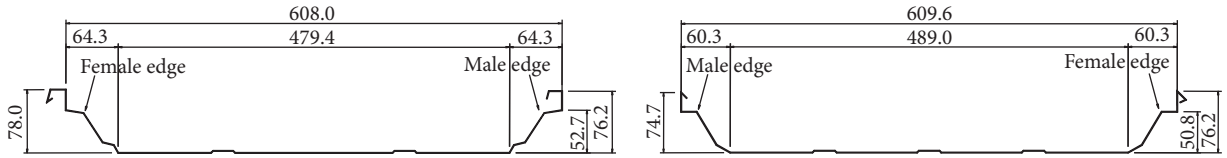

(a) (b)

Figure 1: Dimensions of standing seam roof panels. (a) LSIII roof panel. (b) SS360 roof panel.

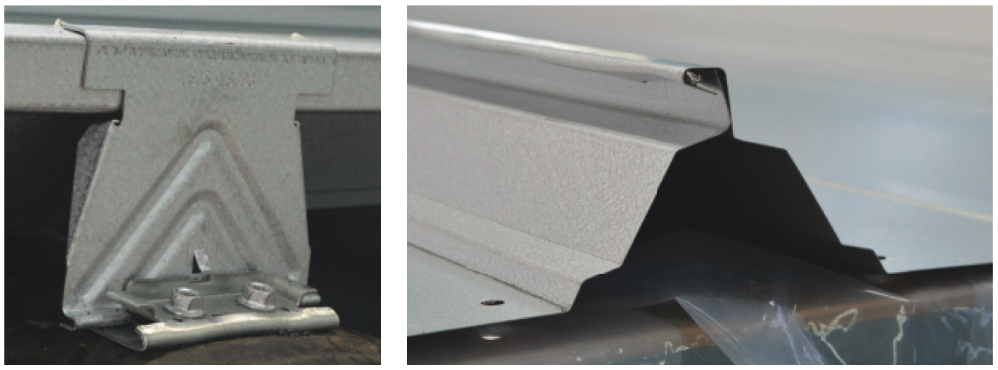

(a) (b)

Figure 2: Connection details of LSIII roof system. (a) LS003 clip. (b) 450° mechanical seam of panel sidelaps.

(a) (b)

Figure 3: Connection details of SS360 roof system. (a) S3PC-1 clip. (b) 360° mechanical seam of panel sidelaps.

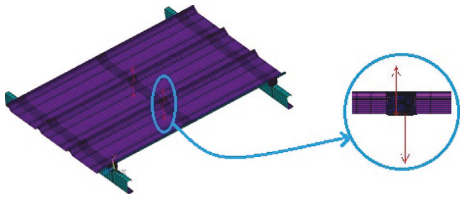

Figure 4: Finite element model for analyzing rotational restraint of standing seam roof systems.

The element types, material models, and boundary conditions were exactly the same as that being used in the full model presented by Luan and Li [21, 22], in which the accuracy of the full model was verified by a comparison between the experimental results and the finite element results, and it is shown that good agreement is achieved between the experimental results and finite element results for the flexural strength and the failure modes. The difference of purlin flexural strength obtained from tests and finite element analysis was smaller than 5%. The load-displacement curves obtained from the finite element analysis were all in great agreement with the test results. Therefore, the finite element models are reliable and can be used for further researches.

3.2. Calculation of Rotational Restraint Rigidity. Using the finite element analysis results, the rotational restraint rigidity (K) provided by the standing seam roof system can be calculated as follows:

$$K = \frac{T}{\theta} = \frac{F \times s}{|\delta_1 - \delta_2|/s}, \quad (1)$$

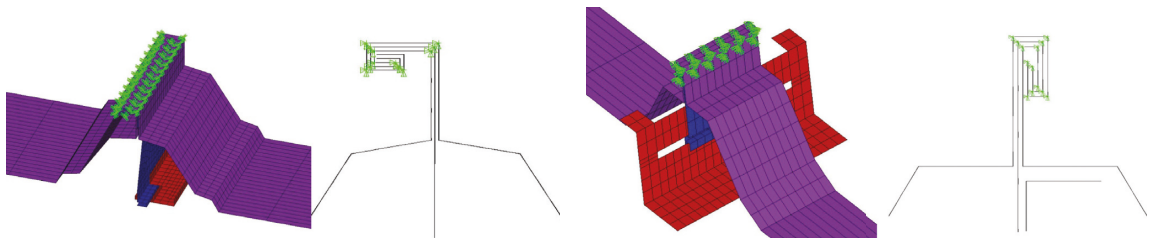

(a) (b)

Figure 5: Connection details of roof panels and clips in finite element models. (a) LSIII roof system. (b) SS360 roof system.

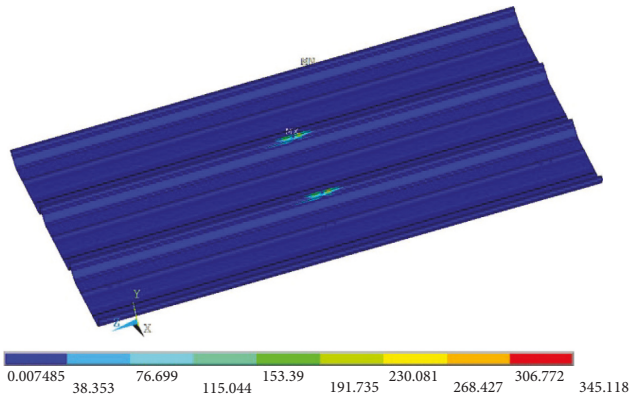

Figure 6: Deformation and stress distribution of the roof panel.

where T is the torque applied on the clip base, θ is the corresponding rotation angle of the clip base, F is the concentrated force applied at the screw points, s is the space between the screws, δ_1 and δ_2 are the corresponding displacements at two screw connection points.

The rotational restraint rigidity on the unit length of purlin (K_{tor}) can be calculated by

$$K_{tor} = \frac{K}{w_{rf}}, \tag{2}$$

where w_{rf} is the width of the standing seam roof panel.

3.3. Finite Element Analysis Results. Using the FE model, the rotational restraints' rigidity to purlins provided by the two types of standing seam roof systems studied in this paper was analyzed. The thickness of the roof panel in both types of roof systems was 0.6 mm, and the panel dimensions and connection details were exactly the same as shown in Figures 1–3. Figure 6 shows the deformation and stress distribution in the roof panel. Figure 7 shows the deformation and stress distribution of two types of clips.

As can be seen, the bending stiffness of the two types of standing seam roof panels is large enough that the clips always fail before roof panels, and the S3PC-1 clip is much easier to deform because the slide tab of which is thinner.

3.4. Analysis of Influence Factors. Theoretically, the rotational restraint rigidity provided by the standing seam roof systems is mainly related to the bending stiffness of roof panels and the sliding performance of clips. The bending stiffness of roof panels generally depends on the thickness and the cross-section profile of the roof panel, and the sliding performance of clips is mainly determined on the thickness of the slide tab. Considering that significant out-of-plane bending deformation of the flat part of the roof panel was observed in the tests, the out-of-plane deflection should also be seen as a factor causing the change of the panel cross-section profile. Therefore, using the finite element model, the influence of different factors on the rotational restraint rigidity provided by the two types of standing seam roof systems was studied. The variables include the relative movement between the slide tab and clip base (S_{tb}), the out-of-plane deflection at mid-point of the roof panel cross-section (D_{rf}), the roof panel thickness (t_{rf}), and slide tab thickness (t_{st}). Analysis results are shown in Figure 8. It is observed that the rotational restraint rigidity mainly depends on the slide tab thickness and the roof panel thickness because the slide tab is the weakest link in the rotational restraint transmission path of the standing seam roof system, and the performance of the mechanical seams connecting the slide tab and the roof panels is closely related to the thickness of roof panel and slide tab. The out-of-plane bending deformation of roof panel and the relative movement between the slide tab and clip base almost have no influence on the rotational restraint rigidity, except for LS003 clip, when the relative movement distance is greater than 40 mm, and half of the slide tab separates from the clip base; thus, the rotational restraint rigidity sharply decreases, however, which is not expected to occur in the actual engineering.

4. Formulae for Rotational Restraint Rigidity

Considering the significant influence on rotational restraint rigidity from the thickness of roof panel and slide tab, further parametric finite element analysis was conducted. Based on the parametric analysis results, formulae for calculating rotational restraint rigidity of the LSIII and SS360 standing seam roof systems were generalized as follows:

$$\text{for LSIII roof system, } K_{tor} = \frac{E}{57} t_{rf}^{0.26} t_{st}^{0.37}, \tag{3}$$

$$\text{for SS360 roof system, } K_{tor} = \frac{E}{50} t_{rf}^{0.32} t_{st}^{0.49}, \tag{4}$$

where t_{rf} is the thickness of the roof panel, t_{st} is the thickness of the slide tab, and E is Young's modulus.

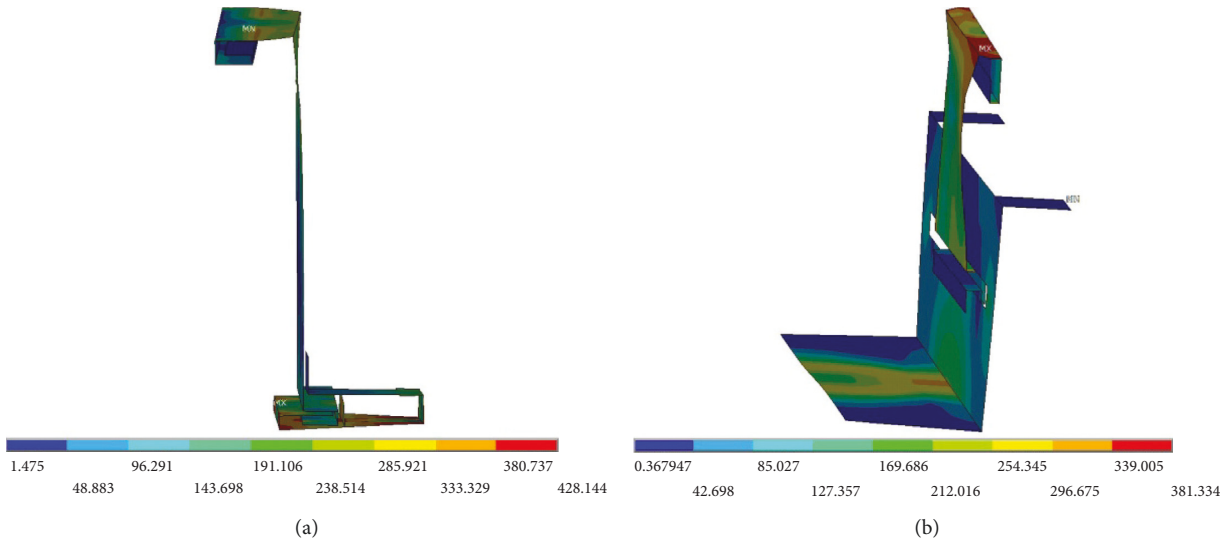

Figure 7: Deformation and stress distribution of sliding clips: (a) LS003 clip and (b) S3PC-1 clip.

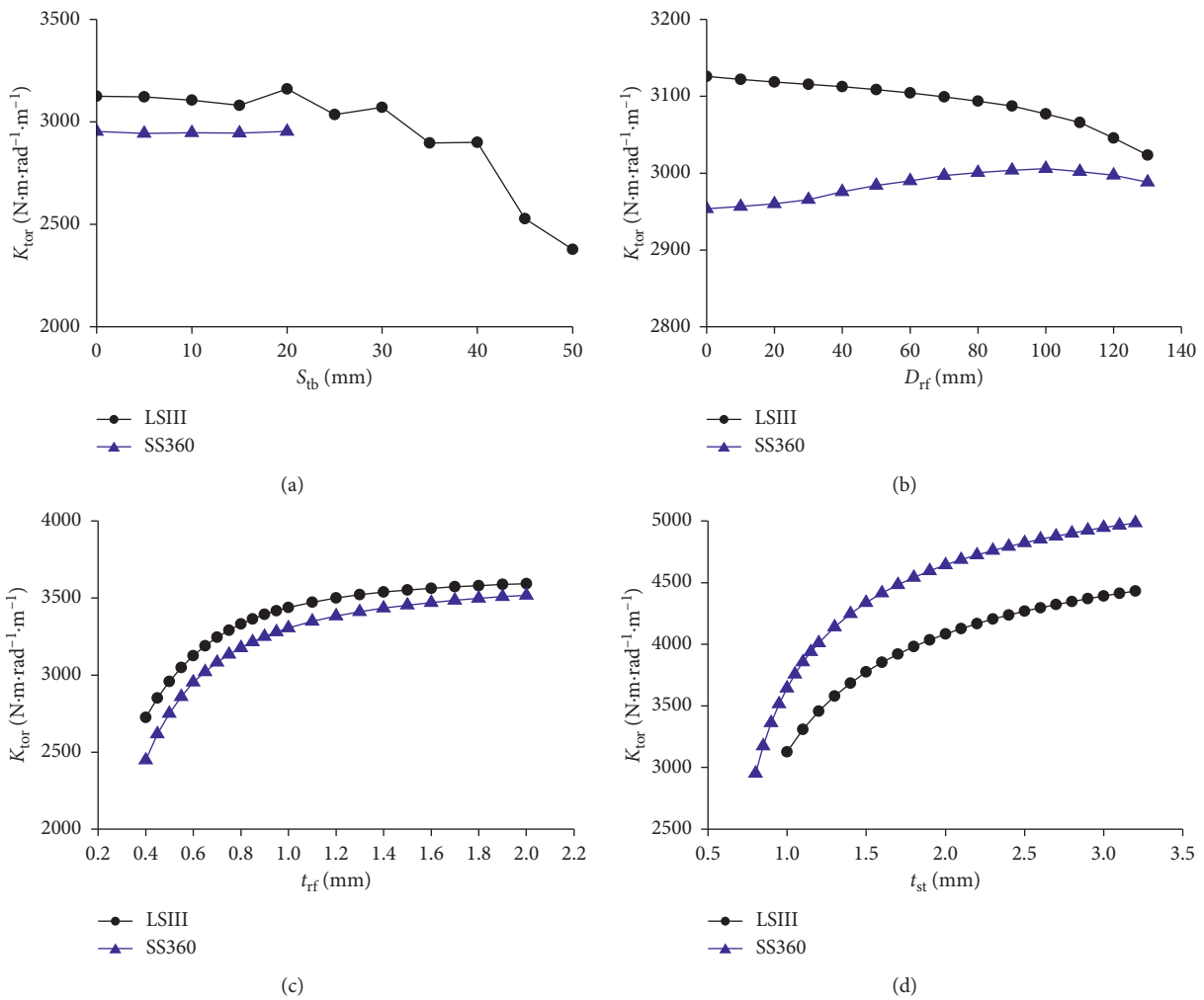

Figure 8: Correlation between the rotational restrain rigidity K_{tor} and factors: (a) between K_{tor} and S_{tb}, (b) between K_{tor} and D_{rf}, (c) between K_{tor} and t_{rf}, and (d) between K_{tor} and t_{st}.

Table 1: Comparison of rotational restraint rigidity calculated by Equation (3) with test result by Liu et al. [20].

Test identification	Purlin section	t_{rf} (mm)	Rotational restraint rigidity ($N{\cdot}m{\cdot}rad^{-1}{\cdot}m^{-1}$)				$(K_z - K_{zt})/K_{zt}$ (%)
			K_{z2}	K_{tor}	K_z	K_{zt}	
ML-8	Z250×60×20×1.5	0.6	424	3165	374	409	−8.50
ML-7	Z250×60×20×2.0	0.6	1006	3165	763	719	6.17
ML-17	Z250×60×20×2.0	0.6	1006	3165	763	712	7.22
ML-20	Z250×60×20×2.0	0.53	1006	3064	757	761	−0.47
ML-13	Z250×60×20×2.5	0.6	1965	3165	1212	1103	9.91
ML-14	Z250×60×20×2.5	0.53	1965	3064	1197	1120	6.90
ML-9	Z200×60×20×1.5	0.6	478	3165	415	447	−7.18
ML-10	Z200×60×20×1.5	0.53	478	3064	413	474	−12.84
ML-11	Z200×60×20×2.0	0.6	1132	3165	834	738	12.97
ML-19	Z200×60×20×2.0	0.6	1132	3165	834	825	1.05
ML-12	Z200×60×20×2.0	0.53	1132	3064	827	722	14.48
ML-18	Z200×60×20×2.0	0.53	1132	3064	827	803	2.93
ML-15	Z200×60×20×2.5	0.6	2211	3165	1301	1214	7.21
ML-16	Z200×60×20×2.5	0.53	2211	3064	1284	1181	8.74
Mean							3.47
COV							8.19

Table 2: Comparison of rotational restraint rigidity calculated by Equation (4) with test result by Liu et al. [20].

Test identification	Purlin section	t_{rf} (mm)	Rotational restraint rigidity ($N{\cdot}m{\cdot}rad^{-1}{\cdot}m^{-1}$)				$(K_z - K_{zt})/K_{zt}$ (%)
			K_{z2}	K_{tor}	K_z	K_{zt}	
HX-1	Z250×70×20×2.5	0.5	1922	2959	1165	1297	−10.16
HX-7	Z250×70×20×2.5	0.6	1922	3136	1192	1391	−14.32
HX-5	Z250×70×20×2.5	0.6	1922	3136	1192	919	29.69
HX-3	Z200×70×20×2.5	0.5	2157	2959	1247	1302	−4.19
HX-2	Z200×70×20×2.5	0.6	2157	3136	1278	1432	−10.76
HX-4	Z200×70×20×2.0	0.6	1104	3136	817	841	−2.89
HX-6	Z200×70×20×2.0	0.6	1104	3136	817	690	18.36
HX-8	Z200×70×20×2.0	0.8	1104	3439	836	680	22.92
Mean							3.58
COV							17.28

To verify the accuracy of the formulae, the rotational restraint rigidity calculated by the proposed formulae was compared with the test results of similar standing seam roof systems by Liu et al. [20]. However, the rotational restraint rigidity obtained from the tests by Liu et al. [20] is total rigidity provided by roof panel, clip, and purlin (K_z), which can be calculated by

$$\frac{1}{K_z} = \frac{1}{K_{z1}} + \frac{1}{K_{z2}}, \tag{5}$$

where K_{z1} is rotational restraint rigidity provided by the roof system, which is the same as K_{tor} in this paper and K_{z2} is rotational rigidity of purlin, which is given by

$$K_{z2} = \frac{\alpha E t^3}{4(1-\nu^2)(3b_1 + b_2 + \alpha h)}, \tag{6}$$

where E is Young's modulus, t is purlin thickness, ν is Poisson's ratio, b_1 is the distance from the inside self-drilling screw to purlin web, b_2 is the space between two self-drilling screws, h is purlin height, and α is the rigidity reduction factor of the top flange of purlin, for LSIII roof system, it is 0.4 and for HX-478 roof system, it is 0.5.

The calculation results of Equations (3) and (4) cannot be compared with the test results directly. Therefore, based on the rotational restraint rigidity of roof system calculated by Equation (3) or Equation (4), using Equations (5) and (6), the total rotational restraint rigidity was calculated and compared with the test results (K_{zt}) by Liu et al. [20]. Table 1 shows the comparison results of LSIII roof system, and it is observed that the calculation results are in good agreement with the test results. The comparison results of SS360 roof system used in this paper and HX-478 roof system tested by Liu et al. [20] are listed in Table 2. It can be seen that the largest difference between the calculation results and the test results reaches about 30%, which is because although the configuration and working mechanism of SS360 roof system and HX-478 roof system are exactly the same, there are still some differences between them, such as the width of roof panel and the dimensions of clips. And, in general, the comparison shows that the rotational restraint rigidity of standing seam roof systems calculated by the formulae proposed in this paper is reliable.

5. Conclusion

In order to study the rotational restraint rigidity provided by two types of standing seam roof systems widely used in China, the finite element model used for analyzing the rotational restraint rigidity of standing seam roof systems was developed based on a test verified full finite element model. The influences of different factors on the rotational restraint rigidity provided by two types of standing seam roof systems were also analyzed. The variables include local deformation of standing seam roof panels, panel thickness, clip tab thickness, and the relative sliding of clip tab and clip base. The analyses showed that the rotational restraint rigidity of standing seam roof systems mainly depended on the roof panel thickness and slide tab thickness. Formulae for calculating rotational restraint rigidity of the LSIII and SS360 standing seam roof systems were also proposed, and the comparison between formulae calculating results and test results showed that the rotational restraint rigidity of standing seam roof systems calculated by the formulae proposed in this paper is reliable.

Data Availability

The datasets generated during the current study are available from the corresponding author on reasonable request.

Conflicts of Interest

The authors declare that they have no conflicts of interest.

Acknowledgments

The research was from the topic of the National Science Foundation of China (no. 51478331) and State Key Laboratory of Disaster Reduction in Civil Engineering (no. SLDRCE14-B-06). The authors are grateful to USAS Building System (Shanghai) Co., Ltd., and ABC Building Systems (China) for supplying the test specimens.

References

[1] N. Celebi, G. Winter, and T. Peköz, "Diaphragm braced channel and Z-section beams," Report No. 344, Department of Structural Engineering, Cornell University, Ithaca, NY, USA, 1972.

[2] M. A. A. Razak and T. Peköz, "Progress report—ultimate strength of co1dFormed steel Z-purlins," Report No. 80-3, Department of Structural Engineering, Cornell University, Ithaca, NY, USA, 1980.

[3] T. Peköz and P. Soroushian, "Behaviour of C- and Z-purlins under wind uplift," in *Proceedings of the 6th International Specialty Conference on Cold-Formed Steel Structures*, pp. 409–429, University of Missouri-Rolla, St Louis, MO, USA, November 1982.

[4] G. J. Hancock, M. Celeban, C. Healy et al., "Tests of purlins with screw fastened sheeting under wind uplift," in *Proceedings of the 10th International Specialty Conference on Cold-formed Steel Structures*, pp. 393–419, University of Missouri-Rolla, St Louis, MO, USA, October 1990.

[5] G. J. Hancock, M. Celeban, and C. Healy, "Tests of continuous purlins under downwards loading," in *Proceedings of the 11th International Specialty Conference on Cold-formed Steel Structures*, pp. 157–179, University of Missouri-Rolla, St Louis, MO, USA, October 1992.

[6] R. A. LaBoube, *Laterally Unsupported Purlins Subjected to Uplift*, Cornell University, Ithaca, NY, USA, 1983.

[7] R. W. Haussler, "Theory of cold-formed steel purlin/girt flexure," in *Proceedings of the 9th International Specialty Conference on Cold-formed Steel Structures*, pp. 255–271, University of Missouri-Rolla, St Louis, MO, USA, November 1988.

[8] H. Wu and C. D. Moen, *Rotational and Translational Stiffness provided by Insulated Metal Panels to Girts and Purlins in Metal Building Wall and Roof Systems*, Virginia Tech, Chennai, India, 2016.

[9] R. A. LaBoube, M. Golovin, D. J. Montague et al., "Behavior of continuous span purlin systems," in *Proceedings of the 9th International Specialty Conference on Cold-Formed Steel Structures*, pp. 191–203, University of Missouri-Rolla, St Louis, MO, USA, November 1988.

[10] C. Zhao, J. Yang, F. Wang, and A. H. C. Chan, "Rotational stiffness of cold-formed steel roof purlin-sheeting connections," *Engineering Structures*, vol. 59, pp. 284–297, 2014.

[11] C. Zhao, *Investigations on Structural Interaction of Cold-Formed Steel Roof Purlin-Sheet System*, University of Birmingham, Birmingham, UK, 2014.

[12] European Commission for Standardization, *EN1993-1-3 Eurocode 3: Design of Steel Structures, Part 1-3: General Rules, Supplementary Rules for Cold Formed Thin Gauge Members and Sheeting*, European Commission for Standardization, Brussels, Belgium, 1996.

[13] K. B. Katnam, R. Van Impe, G. Lagae et al., "A theoretical numerical study of the rotational restraint in cold-formed steel single skin purlin-sheeting systems," *Computers & Structures*, vol. 85, no. 15-16, pp. 1185–1193, 2007.

[14] K. B. Katnam, R. Van Impe, G. Lagae, and M. De Strycker, "Modelling of cold-formed steel sandwich purlin-sheeting systems to estimate the rotational restraint," *Thin-walled Structures*, vol. 45, no. 6, pp. 584–590, 2007.

[15] Y. Guan, *Analytical Study on Rotational Restraint of Sheathing*, Report No. RP08-2, American Iron and Steel Institute, Washington, DC, USA, 2008.

[16] B. W. Schafer, L. C. M. Vieira Jr, R. H. Sangree et al., "Rotational restraint and distortional buckling in cold-formed steel framing systems," *Revista Sul-americana de Engenharia Estrutural*, vol. 7, no. 1, 2011.

[17] AISI S210-10, *North American Standard for Cold-Formed Steel Framing - Floor and Roof System Design*, American Iron and Steel Institute, Washington, DC, USA, 2010.

[18] T. Gao and C. D. Moen, "Extending the direct strength method for cold-formed steel design to through-fastened simple span girts and purlins with laterally unbraced compression flanges," *Journal of Structural Engineering*, vol. 140, no. 6, pp. 145–153, 2013.

[19] T. Gao, *Direct Strength Method for the Flexural Design of Through-Fastened Metal Building Roof and Wall Systems under Wind Uplift or Suction*, Virginia Tech, Chennai, India, 2012.

[20] Y. X. Liu, G. S. Tong, and H. L. Du, "Test and finite element analysis on torsional restrain of corrugated steel sheet to purlin through clips," *Journal of Building Structures*, vol. 35, pp. 116–124, 2014, in Chinese.

[21] W. Luan and Y. Li, "Experimental study on uplift capacity of purlins considering restraints from standing seam roof systems," in *Proceedings of the 11th International Specialty Conference on Cold-Formed Steel Structures*, pp. 157–179, University of Missouri-Rolla, St Louis, MO, USA, October 1992.

[22] W. Luan and Y.-Q. Li, "Experimental investigation on wind uplift capacity of single span Z-purlins supporting standing seam roof systems," *Thin-Walled Structures*, vol. 144, Article ID 106324, , 2019.